Nonrigid Registration of 3-D Free-Hand Ultrasound Images of the Breast

Guofang Xiao, J. Michael Brady, J. Alison Noble*, *Member, IEEE*, Michael Burcher, and Ruth English

Abstract—Three-dimensional (3-D) ultrasound imaging of the breast enables better assessment of diseases than conventional two-dimensional (2-D) imaging. Free-hand techniques are often used for generating 3-D data from a sequence of 2-D slice images. However, the breast deforms substantially during scanning because it is composed primarily of soft tissue. This often causes tissue mis-registration in spatial compounding of multiple scan sweeps. To overcome this problem, in this paper, instead of introducing additional constraints on scanning conditions, we use image processing techniques. We present a fully automatic algorithm for 3-D nonlinear registration of free-hand ultrasound data. It uses a block matching scheme and local statistics to estimate local tissue deformation. A Bayesian regularization method is applied to the sample displacement field. The final deformation field is obtained by fitting a B-spline approximating mesh to the sample displacement field. Registration accuracy is evaluated using phantom data and similar registration errors are achieved with (0.19 mm) and without (0.16 mm) gaps in the data. Experimental results show that registration is crucial in spatial compounding of different sweeps. The execution time of the method on moderate hardware is sufficiently fast for fairly large research studies.

Index Terms—Bayesian regularization, block matching, free-hand, nonlinear registration, soft-tissue deformation, spatial compounding, 3-D ultrasound.

I. INTRODUCTION

ULTRASOUND imaging is a valuable tool for breast disease assessment as images are available in real-time, there is a low health risk to the patient and the cost of acquisition is relatively low. However, conventional two-dimensional (2-D) ultrasound imaging is limited in that the clinician has to mentally transform a sequence of 2-D images into a three-dimensional (3-D) tissue structure in order to make a diagnosis. This demands considerable skill, knowledge, and experience on the part of the clinician. This, in turn, inevitably leads to inaccuracies in assessing morphological features, the sizes, and staging of lesions and in monitoring subtle changes. Moreover, a 2-D image location is often difficult to reproduce in sequential examinations, hampering quantitative serial studies [1].

Three–dimensional ultrasound imaging aims to overcome these limitations. Special 3-D probes, which are able to produce a 3-D image of a volume within the body, are being developed. However, technical challenges, including improvements in spatial resolution, need to be solved before such probes will be useful for routine clinical use. Currently, almost all 3-D ultrasound imaging systems used in clinical practice use conventional 2-D images to construct a 3-D data set. Acquisition of 2-D ultrasound images can be achieved mechanically, with the ultrasound probe moved by a motor in a predefined manner [2]; or *free-hand*, in which the clinician holds the probe and manipulates it freely over the anatomy to be examined [3], [4]. In free-hand acquisition, a localizer is required to record the position and orientation of each 2-D scan in order to reconstruct the 3-D anatomy. The free-hand technique is attractive, not least because it is convenient for the clinician and because of the attainable imaging angle and accessible volume. The work reported in this paper is based on sequences of free-hand B-mode scans acquired using a conventional 2-D transducer.

In 3-D free-hand ultrasound imaging, the clinician normally sweeps the probe across the anatomy of interest. Often two or more sweeps are needed to obtain a complete volume. The combination of the sweeps is called *spatial compounding*, which also helps reduce speckle noise when sweeps are taken along different directions [5]. The soft nature of the breast causes a problem here: while the clinician sweeps the probe across the breast surface, it deforms easily and the deformation differs substantially for each scan acquired. For each sweep, through careful scanning, the anatomy inside the breast can undergo small deformation. However, if several such sweeps are compounded, the reconstructed volume typically appears blurred because of tissue mis-registration [Fig. 1(a)]. This problem can be reduced by immobilizing the breast with an appropriate device. For instance, a modified mammography unit was used in [2], [6]. However, such a device causes discomfort to the patient (although the compression used is typically not as strong as used in X-ray mammography). Further, when the breast is compressed in this way, lesions near the chest wall may not be accessible.

Ideally, 3-D scans should be performed with minimal constraints on scanning conditions. In our study, scanning is done with only minor modifications to the standard 2-D scanning protocol. Image processing techniques are used to solve image mis-registration as illustrated in Fig. 1(b). Consider one sweep to be the reference image. The method aligns the second sweep to the first and then compounds them together. The problem then reduces to how to align two such volumes, possibly with gaps in each sweep. This is the problem addressed in this paper.
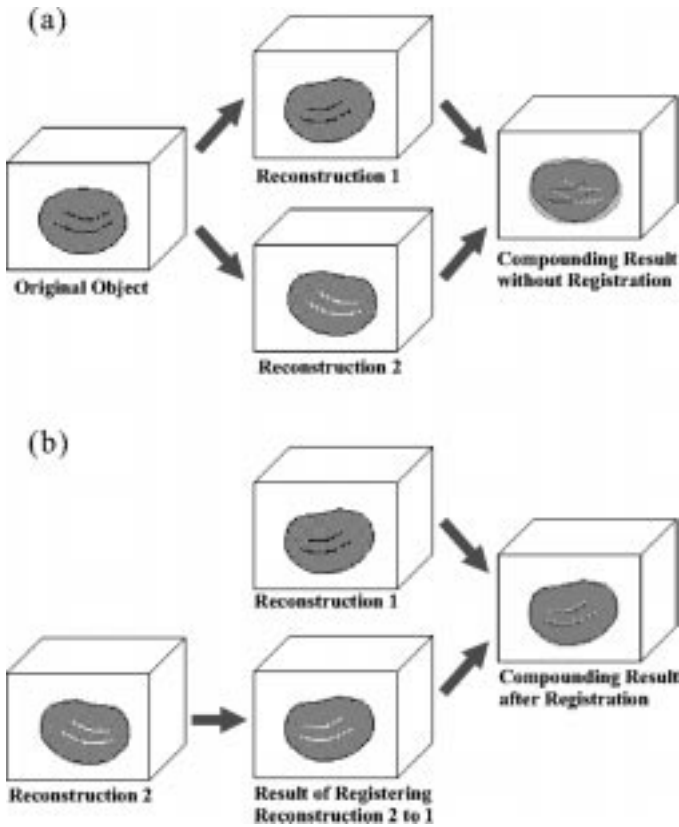
Fig. 1. Spatial compounding of two sweeps (a) without and (b) with registration.

The paper is organized as follows. Section II first explains why the particular registration method was chosen for the study, given the broad range of contending approaches. Then, the nonlinear registration algorithm, consisting of three main parts, is described in detail. Some considerations specific to applying the general algorithm to 3-D free-hand data are then discussed. Experimental results are presented in Section III. Section IV concludes the paper. An early and much shorter version of this work was presented in [7].

II. METHOD

A. Determining the Registration Method

A wide range of methods have been developed for registration, each suited to certain types of data and problems [8], [9]. It remains the case that the choice of an appropriate registration method has to be determined for each specific application. For our work, for example, it is clear that the required transformation is nonlinear (more precisely, nonaffine). According to the type of information in the images to be registered, published methods can be divided into two main classes.

- *Feature-based methods.* This type of method relies on a preprocessing step (image feature detection) in order to identify various anatomical structures as features. Features that have been used with success include points, edges, surfaces, or volumes. Such structures are then matched and the transformation that best superimposes them is found. Clearly, registration accuracy of this category of methods depends on the reliability and sta-

bility of feature extraction. In early work on ultrasound image registration, for example [5], this approach was investigated with limited success due to the problem of reliably detecting image features. Due to the difficulty in segmenting ultrasound images we have not used this approach.

- *Voxel property-based methods.* In this type of method, there is no need to extract features prior to registration. Instead, the voxels themselves are used. Either a voxel similarity measure between different images is defined and the transformation is optimized to maximize this measure, or some kind of force is formed and it drives one of the images to deform into the other. This is the approach used in this paper.

In the literature, voxel property-based algorithms have mostly been applied to estimate rigid or affine transformations [9]. The transformation parameters (translation, rotation and scaling) are optimized to maximize a voxel similarity measure between different images. For nonaffine registration, several notable general voxel property-based algorithms include Christensen's viscous fluid flow model [10], Bro-Nielsen's fast fluid registration [11], Thirion's "demons' algorithm [12], and the spline-based free-form deformation (FFD) method of Rueckert *et al.* [13]. Specifically, in the ultrasound literature, Aiger *et al.* [14] has proposed using a gradient-based method and Krucker *et al.* [15] uses a thin-plate spline warping transformation. However, all the above approaches depend on the gradient computation of voxel intensities which is problematic in 3-D free-hand ultrasound data where there are typically (and in some cases significant) gaps between the scans in volumes reconstructed from individual B-scan sweeps (see Fig. 10). This, together with the noisy nature of ultrasound images hinders the application of such methods in practice. Filling the gaps by intensity interpolation has been proposed as a solution but this introduces error, particularly for larger gaps. Another solution might be to increase the voxel size, that is reduce the volume resolution in order to eliminate gaps. In practice, this results in substantial blurring of the texture of (breast) tissues, which is undesirable, particularly for a voxel property-based method. Original contributions of this paper are to propose an alternative solution to this problem which does not involve gradient computation and to accommodate gaps in a novel way using a block-matching registration method [16], [17].

In block-matching registration, the reference image is sampled at a set of grid points. Each sample is a block of voxels centred on a grid point. The block is moved to several positions within a 3-D search window, where within the block some local voxel similarity measure is computed between the two images. For each sample, the position that maximizes the local voxel similarity measure under some regularization constraint is found and used to form the deformation field of the image.

Let I_1 and I_2 be two images and U be the deformation field. The energy function for local voxel similarity can be define as

$$E_{\text{similarity}}(U) = -\sum_{\mathbf{x} \in \mathcal{S}} (W_{\mathbf{x}} \cdot I_1) \otimes (W_{\mathbf{x}} \cdot (U \circ I_2)) \quad (1)$$

where $\otimes$ denotes the operator for measuring voxel similarity, $U \circ I_2$ is the transformed version of I_2, and $W_{\mathbf{x}}$ is a window

function centred at sample site $\mathbf{x}$, $\mathbf{x} \in \mathcal{S}$, $\mathcal{S}$ being the sample set. $W_{\mathbf{x}}$ can be, for example, a uniformly dense block [18], [19], or a uniformly dense or weighted (for instance Gaussian-weighted) sphere [17].

The deformation field is often assumed to be smooth and *regularization* applied. Regularization can be formulated as an energy function to be minimized. For example, the commonly used

$$E_{\text{regularization}}(U) = \int \left\| \frac{\partial U}{\partial \mathbf{x}} \right\|^2 d\mathbf{x} \tag{2}$$

penalizes large gradients in the deformation field. Regularization can also be effected by other means. For instance, Bayesian regularization is used in [18] and a simple smoothing step is applied to the deformation field in [16].

Minimization of the energy function may be done through simple exhaustive search [18], [19], or by classic optimization strategies such as Simplex optimization [16] or gradient descent [17]. We used exhaustive search because of its simplicity and speed.

The spacing of the sampling grid is typically larger than the image voxel size, that is, block sampling is sparse. Some kind of interpolation or approximation is then needed to assign a displacement vector to every voxel. This considerably reduces computation time compared to directly computing a displacement vector for every voxel, especially for 3-D images.

We chose to use a block matching scheme for nonlinear registration, because it is voxel property-based and gradient computation is not needed (which is problematic when sparse data is available). In particular, the proposed method is based on the Bayesian nonlinear registration algorithm proposed in [18] as described below.

B. The Nonlinear Bayesian Registration Algorithm

The nonlinear Bayesian registration algorithm [18] consists of three main parts: computing the similarity scores of sample displacements via block matching, Bayesian regularization of the displacements and generating the final deformation field. We review the steps in the next subsections.

1) Computing Similarity Scores of Sample Displacements: The reference image is sampled at a set of 3-D grid points. Each sample is a block of voxels centred on a grid point. Each block is then moved to several positions within a search window. Fig. 2 is a 2-D illustration of the idea. At each position, an intensity correlation coefficient score, CC, between the block and the corresponding block in the floating image is computed as

$$CC = \frac{\sum_{\mathbf{x}} (I_1(\mathbf{x}) - \mu_1)(I_2(\mathbf{x}) - \mu_2)}{\sqrt{\sum_{\mathbf{x}} (I_1(\mathbf{x}) - \mu_1)^2} \cdot \sqrt{\sum_{\mathbf{x}} (I_2(\mathbf{x}) - \mu_2)^2}}. \tag{3}$$

Here, $I_1(\mathbf{x})$ and $I_2(\mathbf{x})$ are the intensity values at voxel $\mathbf{x}$ in the two corresponding blocks, respectively, and μ_1 and μ_2 are the corresponding mean intensities. Thus, each sample has a 3-D map of scores for all possible displacements.

The search window size is determined by the expected likely deformation in the image. The spacing of the sampling grid determines the resolution of the displacement field. A smaller grid
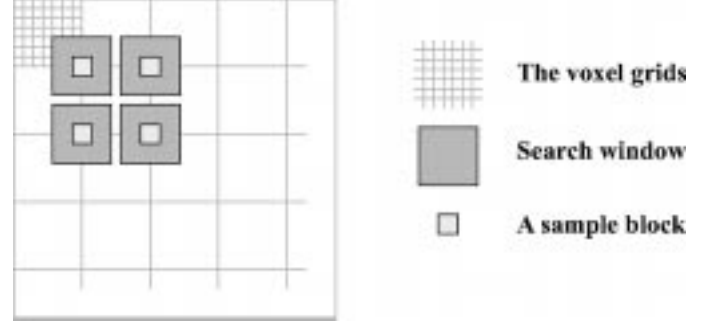

Fig. 2. Two-dimensional illustration of the block matching scheme.

spacing provides higher spatial resolution and resolves more variable displacement fields; but at the expense of increased computation time. There is also a tradeoff in choosing the size of the blocks. Smaller blocks capture more localized displacement information, but at the same time are more susceptible to noise as they carry less information. Larger blocks are more unique. This increases matching accuracy. However, the spatial resolution of the displacement field degrades because of the underlying assumption that voxels inside one block have identical displacement. A multilevel block matching strategy such as used in [20], could be used to combine the advantages of both large and small matching blocks. In our work, a single-level block matching scheme has been used and as will be discussed in Section II-C we employ a novel anisotropic block sampling and searching scheme to resolve the complex deformation between B-scans and to keep the deformation smooth within each B-scan.

2) Bayesian Regularization: For each block, the maximum similarity score does not necessarily correspond to the best displacement, partly because of noise and partly because of the *aperture problem* [21]. A regularization step is necessary and this is achieved by taking into account the influence of the displacements of neighboring sites. If the initial similarity scores are normalized, they can be considered as estimates of the prior probabilities of those displacements

$$P(\mathbf{u}_{\mathbf{x}}) = \frac{C_{\mathbf{x},\mathbf{u}}}{\sum_{\mathbf{u}} C_{\mathbf{x},\mathbf{u}}} \tag{4}$$

where $\mathbf{u}_{\mathbf{x}}$ denotes the displacement $\mathbf{u}$ of the sample block at location $\mathbf{x}$ and $C_{\mathbf{x},\mathbf{u}}$ the similarity score of $\mathbf{x}$ with displacement $\mathbf{u}$. Bayes' rule can be used to obtain the posterior probability of each displacement

$$P(\mathbf{u}_{\mathbf{x}}|\mathbf{u}_{\mathcal{N}_{\mathbf{x}}}) = \frac{P(\mathbf{u}_{\mathcal{N}_{\mathbf{x}}}|\mathbf{u}_{\mathbf{x}}) P(\mathbf{u}_{\mathbf{x}})}{P(\mathbf{u}_{\mathcal{N}_{\mathbf{x}}})} \tag{5}$$

where $\mathcal{N}_{\mathbf{x}}$ denotes the sample blocks adjacent to $\mathbf{x}$. $P(\mathbf{u}_{\mathcal{N}_{\mathbf{x}}})$ serves as a normalizing constant.

To use (5), a model of $P(\mathbf{u}_{\mathcal{N}_{\mathbf{x}}}|\mathbf{u}_{\mathbf{x}})$ needs to be defined. It is assumed that, given a displacement $\mathbf{u}$ at $\mathbf{x}$, the probabilities of displacement $\mathbf{u}$ at different neighboring sites are independent of one another. It follows that:

$$P(\mathbf{u}_{\mathcal{N}_{\mathbf{x}}}|\mathbf{u}_{\mathbf{x}}) = \prod_{\mathbf{x}' \in \mathcal{N}_{\mathbf{x}}} P(\mathbf{u}_{\mathbf{x}'}|\mathbf{u}_{\mathbf{x}}) \tag{6}$$

where $P(\mathbf{u}_{\mathbf{x}'}|\mathbf{u}_{\mathbf{x}}), \mathbf{x}' \in \mathcal{N}_{\mathbf{x}}$ is the probability that $\mathbf{x}'$, a neighbor of $\mathbf{x}$, has the displacement $\mathbf{u}$, given that $\mathbf{x}$ has displacement $\mathbf{u}$. This is modeled as

$$P(\mathbf{u}_{\mathbf{x}'}|\mathbf{u}_{\mathbf{x}}) = \max_{\mathbf{v}} \left(P(\mathbf{v}_{\mathbf{x}'}) \exp\left(-\frac{(\mathbf{v}-\mathbf{u})^2}{2\sigma_{\mathbf{u}}^2}\right) \right) \quad (7)$$

where $\|\mathbf{v} - \mathbf{u}\| < \epsilon$, ϵ being a threshold. $P(\mathbf{v}_{\mathbf{x}'})$ is the probability of displacement $\mathbf{v}$ at $\mathbf{x}'$, $\mathbf{v}$ being a displacement similar to $\mathbf{u}$ ($\|\mathbf{v} - \mathbf{u}\| < \epsilon$). $\sigma_{\mathbf{u}}$ is a constant.

Taking logarithms of (5) and making use of (6) and (7), the update equation becomes

$$P_{\log}(\mathbf{u}_{\mathbf{x}}|\mathbf{u}_{\mathcal{N}_{\mathbf{x}}}) = \sum_{\mathbf{x}' \in \mathcal{N}_{\mathbf{x}}} \max_{\mathbf{v}} \left(P_{\log}(\mathbf{v}_{\mathbf{x}'}) - \left(\frac{(\mathbf{v}-\mathbf{u})^2}{2\sigma_{\mathbf{u}}^2}\right) \right)$$
$$+ P_{\log}(\mathbf{u}_{\mathbf{x}}). \quad (8)$$

(Note that $P(\mathbf{u}_{\mathcal{N}_{\mathbf{x}}})$ does not appear here because it is a constant). Equation (8) is applied for a heuristically determined number of iterations. The resulting displacement field U is obtained using the *maximum a posteriori* (MAP) principle: for each sample block, the displacement corresponding to the maximum posterior probability is the estimate of its displacement

$$U(\mathbf{x}) = \arg\max_{\mathbf{u}_{\mathbf{x}}} P(\mathbf{u}_{\mathbf{x}}|\mathbf{u}_{\mathcal{N}_{\mathbf{x}}}). \quad (9)$$

3) Generating the Deformation Field: So far, we have obtained the displacement vectors of a set of sample blocks in the image. A deformation field is obtained by fitting a cubic tensor product B-spline approximating mesh of the form

$$u(x,y,z) = \sum_{i=0}^{n_x-1} \sum_{j=0}^{n_y-1} \sum_{k=0}^{n_z-1} \alpha_{i,j,k} B_i^x(x) B_j^y(y) B_k^z(z) \quad (10)$$

$$v(x,y,z) = \sum_{i=0}^{n_x-1} \sum_{j=0}^{n_y-1} \sum_{k=0}^{n_z-1} \beta_{i,j,k} B_i^x(x) B_j^y(y) B_k^z(z) \quad (11)$$

$$w(x,y,z) = \sum_{i=0}^{n_x-1} \sum_{j=0}^{n_y-1} \sum_{k=0}^{n_z-1} \gamma_{i,j,k} B_i^x(x) B_j^y(y) B_k^z(z) \quad (12)$$

to the set of sample displacement vectors [22]. Using the x coordinate as an illustration, the meaning of the notation is: n_x is the number of control points of the B-spline in the x direction, α is the 3-D matrix of the x coordinates of the control points, and B_i^x is the ith cubic B-spline basis function. Regular 3-D grid points are used for the knots.

Matrices α, β, and γ are found by minimizing the energy function

$$E^x(u) = E_{\text{close}}^x(u) + \lambda E_{\text{smooth}}^x(u) \quad (13)$$

where λ is a weighting coefficient and $E_{\text{close}}^x(u)$ measures the closeness of the fitting

$$E_{\text{close}}^x(u) = \sum_{i=1}^{N} \left(u\left(x_1^i, y_1^i, z_1^i\right) - x_2^i \right)^2. \quad (14)$$

Here, (x_1, y_1, z_1) and (x_2, y_2, z_2) are the matching block locations in the two images and N is the number of the blocks.

$E_{\text{smooth}}^x(u)$ measures the smoothness of the fitting and takes the form

$$E_{\text{smooth}}^x(u) = \int \int \int_{\mathbb{R}^3} \left(u_{xx}^2 + u_{yy}^2 + u_{zz}^2 + 2u_{xy}^2 + 2u_{yz}^2 + 2u_{xz}^2 \right). \quad (15)$$

The minimization is performed with respect to each of the parameters $\alpha_{i,j,k}$, $\beta_{i,j,k}$, and $\gamma_{i,j,k}$ using a conjugate gradient descent method.

4) The Complete Nonlinear Registration Algorithm: The complete nonlinear registration algorithm is summarized as follows.

```
1. Compute the correlation coefficient scores
for a set of blocks sampled on a regular grid,
for all possible displacements within a search
window and normalize them as the prior proba-
bilities of matching (4).
2. For each sample block, compute the poste-
rior probability of each displacement, given
the displacement estimates of its surrounding
blocks (8).
3. Renormalize the estimated probabilities. Go
to Step 2 unless the required number of itera-
tions have been completed.
4. Find the displacement field of the sample
blocks, by taking as the displacement estimate
the displacement corresponding to the maximum
posterior probability for each sample (9).
5. The deformation field is obtained by a
B-spline approximation mesh fitting (10)-(12).
```

C. Special Considerations for 3-D Free-Hand Data

1) Empty Voxels: As stated previously, in each 3-D free-hand ultrasound volume, there are inevitably gaps between the scans. Hence, there will be empty voxels in the 3-D sample blocks and their search windows. These empty voxels contain unknown information (rather than zero values) and this needs to be taken into account when computing similarity scores. To solve this problem, if a sample block contains mostly empty voxels (in the experiments described here, we used a figure of 50%), it is marked "uncertain" and the prior probabilities of all its possible displacements are set to be the same value. Its displacement will be determined by the displacements of neighboring sample blocks according to the posterior updating equation (6). This also applies to "flat" sample blocks (characterized by low intensity variance) such as those inside a cyst. If a sample block is not "uncertain," but its corresponding blocks at some positions within the search window mostly contain empty voxels, then the prior probabilities of these displacements are set as "uncertain." In our implementation, they are assigned with the average value of the prior probabilities of other displacements within the search window that have certain (i.e., valid) values.

2) Anisotropic Sampling and Searching: In most block matching methods, the sample blocks and search windows are
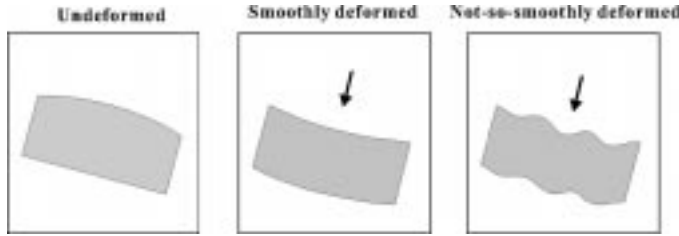
Fig. 3. Reconstructed volumes with different extent of deformation. The arrow points to the direction of the applied force from the probe.

Fig. 4. (a) Isotropic and (b) anisotropic block sampling. The hatching indicates the B-scan planes.

spatially isotropic, that is, they are squares for 2-D images and cubes for 3-D images. We have found this choice acceptable only when the deformation varies very smoothly across the B-scans [Fig. 3(b)]. However, if the deformation field fluctuates [Fig. 3(c)], we have found that registration results are often unsatisfactory. The latter case often happens in free-hand scanning of the breast, because it is a very soft organ. In fact, we have found such fluctuations in almost half of all the sweeps we have acquired in the Oxford breast clinic (Oxford, U.K.). When cubic blocks are used, it is implicitly assumed that the voxels inside, which are from a number of different B-scans, all have the same displacement. Also, when block searching is carried out isotropically in space, the deformation is implicitly assumed to be isotropic. However these assumptions are not true here since in free-hand scanning, the B-scans are acquired independently. Consequently they deform independently and the deformation occurs mainly within each B-scan plane (the out-of-plane deformation is not observed and is assumed to be negligible[1]). This suggests that the block sampling and searching should be anisotropic.

We take advantage of the fact that, in free-hand imaging, the B-scan sweeps are usually taken across a flat area of the anatomy of interest and the B-scans in each sweep are very close to parallel. A new sampling scheme has been developed, as illustrated in Fig. 4. Consider reorienting the coordinate system so that the z axis aligns with the average normal of the B-scans in the floating image. Then the B-scans in the floating image are all approximately parallel to the x–y plane of the coordinate system. The sample blocks are "square tablets,", having equal dimensions in the x and y directions but thinner in the z direction, while the sampling grid is denser in the z direction than in the other two directions. Block matching is limited to the x and y directions, under the assumption that deformation of the floating image occurs mainly within each B-scan plane. This also reduces the computation time significantly. Accordingly, in Bayesian regularization, only blocks in the same search plane influence each other. More explicitly, for each sample block, the eight nearest-neighbors in the x–y plane are considered. In the final B-spline fitting, more control points are used in the z direction than in x and y in order to allow more deformation in this direction. Such an anisotropic sampling and searching scheme enables complex deformation changes between B-scans to be resolved while maintaining smoothness within each B-scan.

[1]This assumption is valid provided there is no tissue "pull." We have found this to be true experimentally if sufficient coupling gel is used on the breast and the radiologist scans carefully/slowly.
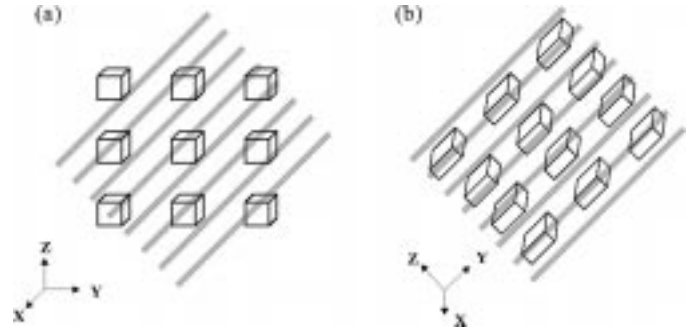
III. EXPERIMENTS

Data was acquired using a 3-D free-hand ultrasound imaging system consisting of an ultrasound scanner (HP SONOS 5500, 10-MHz linear-array transducer for the *in vitro* experiment and Esaote AU4 Idea, 7.5-MHz linear-array transducer for the *in vivo* experiments), a Polaris optical tracking system (Northern Digital Inc., Waterloo, ON, Canada) with a 90° field-of-view and aroot-mean-square error of 0.35 mm and a personal computer equipped with a Matrox Meteor frame grabber which grabbed images from the scanner at a rate of ten frames/s. A single-point calibration method based on imaging a novel calibration object and automatic, fast, and accurate feature detection was used for system calibration [23]. Scanning was performed by repeatedly sweeping the transducer across the region of interest. 2-D B-scans in each sweep were reconstructed into a regular 3-D volume according to their (3-D) position and orientation. The intensity of each voxel was calculated as the distance-weighted sum of intensities of the pixels that fell into a voxel.

A. In Vitro Experiment

A box of gelatin consisting of three layers of different concentrations (Fig. 5) was constructed, mimicking the layered structure of the breast anatomy typically seen with ultrasound imaging. The top two layers were made uneven in order to generate blob-like objects mimicking the appearances of ducts, lesions and etc. inside the breast. Talcum powder was added to increase back-scattering.

After the gelatin was well set, water was poured in to form a fourth layer on top of the gelatin. Scanning was performed with the front surface of the ultrasound probe immersed in the water layer, but not touching the surface of the gelatin. Hence, it is justifiable to assume that for each sweep taken, there was no deformation of the gelatin. In other words, any two of the reconstructed sweeps were initially well-registered to each other.

Two sweeps were acquired along two slightly different directions (about 5° apart), with the probe moving very slowly to ensure that there were no gaps in the reconstructed images [Fig. 6(a) and (b)]. Approximately 300 images were used to reconstruct each of the two sweep volumes. The following artificial deformation was then applied to the floating image: for each x–y plane, a shift $\triangle y = 3\sin(z/5)$ in the y direction was made for all the voxels in it [Fig. 6(c)]. The nonlinear registration algorithm was then applied to estimate the (known) deformation.
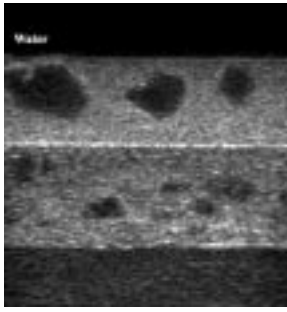
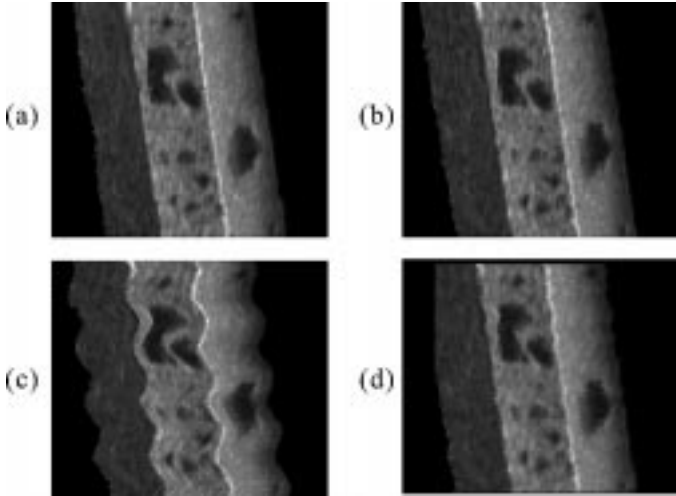Fig. 5. Two-dimensional B-scan of the gelatin phantom.

Fig. 6. Registration experiment on the gelatin phantom, with complete data. (a) A resliced view of the reference image. (b) The same resliced view of the original floating image. (c) The distorted floating image. (d) The recovered floating image.
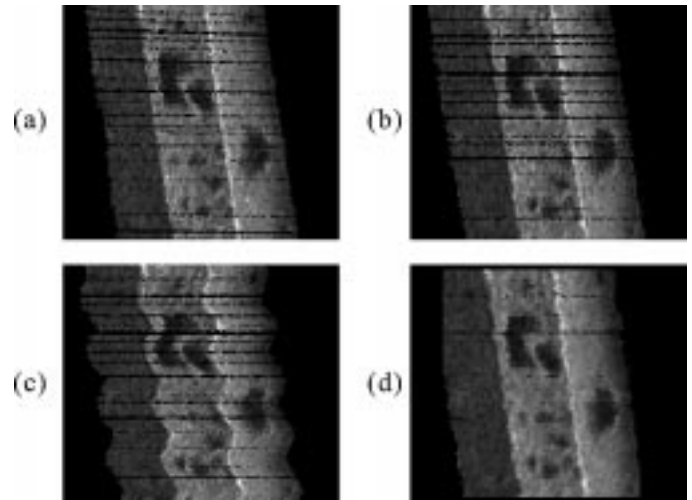

Fig. 7. Registration experiment on the gelatin phantom, with incomplete data. (a) A resliced view of the reference image. (b) The same resliced view of the original floating image. (c) The distorted floating image. (d) The recovered floating image.
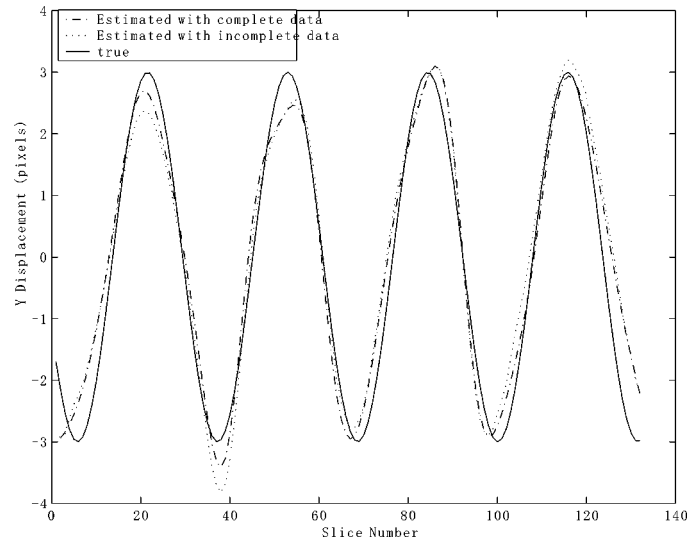

Fig. 8. Plot of the mean value of the y displacements estimated for all the voxels in each x–y plane, with complete and incomplete data.

The two volumes [Fig. 6(a) and (c)] were both $127 \times 160 \times 136$ voxels in size, with a voxel size of 0.4 mm in each of the x, y and z directions. The reference image was sampled at 3-D grid points with a spacing of six, six, and two voxels in the x, y, and z directions, respectively. The sample block size used was $11 \times 11 \times 5$ voxels and the search windows 21×21 (in the x–y plane only). The B-spline mesh had eight, eight, and 24 control points in x, y, and z directions, respectively. The algorithm was run with ten iterations of Bayesian regularization. The mean value of the y displacements estimated for all the voxels in each x–y plane is plotted in Fig. 8. A mean registration error of 0.40 voxels (0.16 mm) was obtained.

We acquired two further sweeps with the probe moving at a typical speed that a clinician would use for *in vivo* scanning. Approximately 60 images were used to reconstruct each of the two sweep volumes and gaps appeared in the reconstructed images [Fig. 7(a) and (b)]. The same operations as described above were performed and a similar mean registration error (0.47 voxels or 0.19 mm) was obtained. From this we conclude that the new registration method successfully copes with the gaps in sweeps.

B. In Vivo Experiments

In vivo 3-D free-hand scanning was performed on patients with their consent at the Breast Care Unit, Churchill Hospital
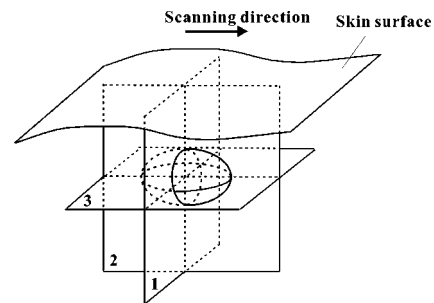

Fig. 9. Three-orthogonal-plane reslicing of 3-D ultrasound raw intensity data.

(Oxford, U.K.) Sufficient ultrasound coupling gel was spread on the breast skin surface to ensure good contact and smooth scanning. The clinician swept slowly across the region of interest several times, each time in a different direction and with the breast deformed as little as possible. The acquisition time
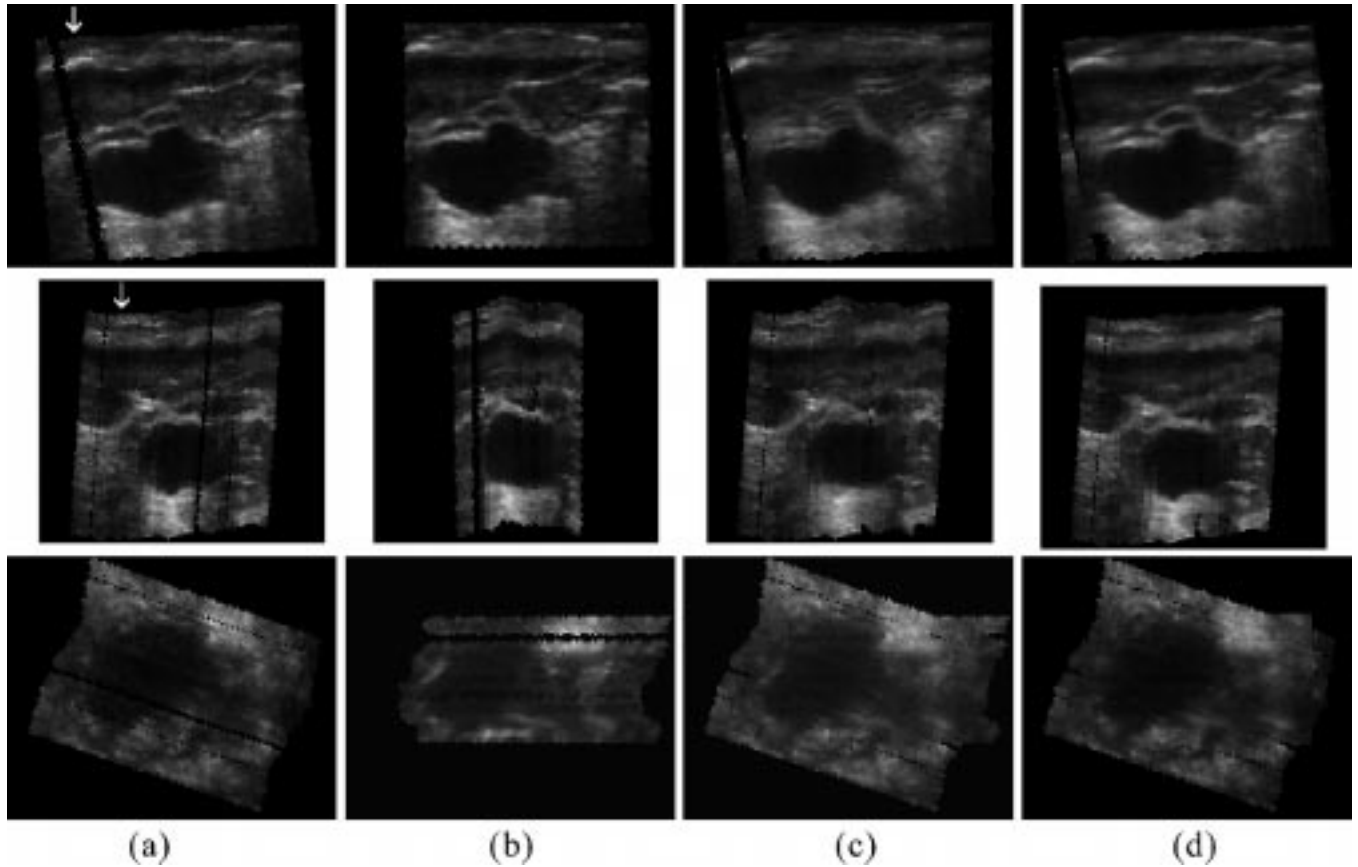
Fig. 10. Three-orthogonal-plane view of steps in 3-D nonlinear registration of cyst data By column, (a) Sweep 1 (reference image), (b) Sweep 2 (floating image), (c) sum of Sweeps 1 and 2 without registration, and (d) sum of Sweep 1 and 2 with registration.

was less than 2 min. In order to minimize the effects of respiratory motion, patients were asked to breathe shallowly.

Fig. 10 shows the registration of two reconstructed sweeps of a breast cyst (image size $149 \times 154 \times 121$ voxels, with an isotropic voxel size of 0.4 mm^3). The top, middle, and bottom rows show three resliced, orthogonal planes (corresponding to Planes 1, 2, and 3, respectively, as illustrated in Fig. 9) intersecting at one fixed point in space in the middle of the cyst. The cyst cross-sections in the top row are about 18 mm wide. Columns (a) and (b) show three-orthogonal-plane views of Sweep 1 (the reference image) and Sweep 2 (the floating image), respectively. The white arrows in Column (a) point to the reconstructed breast surface. For Sweep 2, due to the reorientation of the coordinate system, the top image is in a plane approximately parallel to its B-scans. The middle image is in a plane approximately perpendicular to the B-scans, in which the fluctuating nature of the scanning surface of Sweep 2 is clearly seen. The algorithm was run with the same anisotropic sampling, searching and B-spline fitting parameters as in the *in vitro* experiment. The total algorithm runtime was about 6 min on an Intel Pentium III/700-MHz CPU. Columns (c) and (d) show the compounding results of Sweep 1 and Sweep 2 before and after registration, respectively. It is clear that the boundary of the cyst and the background texture are blurred using compounding without registration (c), while they are well preserved if registration is performed first (d).

The second example involves registering and compounding two sweeps of a breast fibroadenoma. Fig. 11 shows images resliced by a plane approximately orthogonal to the B-scans of the floating image. The white arrows in Fig. 11(a) and (b) point to the reconstructed breast surface. The algorithm was run with the same anisotropic sampling, searching and B-spline fitting parameters as in the previous experiments. Registration clearly gives better definition to tissue structures and a smoother image appearance. It is interesting to note that the relatively hard fibroadenoma seems to have deformed substantially. In fact, it was not the fibroadenoma itself, but the soft tissue above and beneath it that was deformed. Neither of the two reconstructed sweeps reflect the true (un-deformed) shape of the fibroadenoma. This is because each 2-D B-scan in a sweep was acquired with the fibroadenoma moved downwards by an amount related to the probe pressure at that place. However, during free-hand scanning the pressure may be different for each sweep. On-going work in our laboratory is investigating methods of recovering the un-deformed shape of soft tissue masses using an instrumented ultrasonic probe [24].

IV. CONCLUSION

A fully automatic algorithm for 3-D nonlinear registration of free-hand ultrasound data has been presented. It uses a block
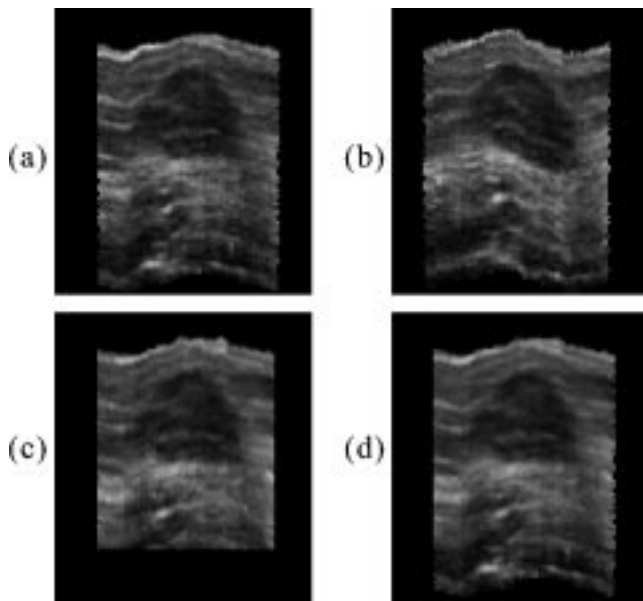
Fig. 11. Registration and compounding of two sweeps of a breast fibroadenoma. (a) Sweep 1 (the reference image). (b) Sweep 2 (the floating image). (c) The result of registering Sweep 2 to Sweep 1. (d) Compounding of Sweep 1 and 2 after registration.

matching scheme and local statistics to capture local tissue deformation. In *in vivo* experiments the algorithm coped with significant deformations of the breast that are frequently encountered in 3-D free-hand scanning. The clinician and the patient behaved almost as they would normally in a clinical examination during data acquisition. The runtime of the algorithm is reasonable for fairly large research studies.

ACKNOWLEDGMENT

REFERENCES

[1] A. Fenster and D. B. Downey, "3-D ultrasound imaging: A review," *IEEE Eng. Med. Biol. Mag.*, vol. 15, no. 6, pp. 41–51, 1996.

[2] P. L. Carson, A. P. Moskalik, A. Govil, M. A. Roubidoux, J. B. Fowlkes, D. Normolle, D. D. Adler, J. M. Rubin, and M. Helvie, "The 3D and 2D color flow display of breast masses," *Ultrasound Med. Biol.*, vol. 23, pp. 837–849, Nov.-Dec. 1997.

[3] P. R. Detmer, G. Bashein, T. Hodges, K. W. Beach, E. P. Filer, D. H. Burns, and D. E. Strandness, "3-D ultrasonic image feature localization based on magnetic scan-head tracking: *In vitro* calibration and validation," *Ultrasound Med. Biol.*, vol. 20, no. 9, pp. 923–936, 1994.

[4] Y. Sato, M. Nakamoto, Y. Tamaki, T. Sasama, I. Sakita, Y. Nakajima, M. Monden, and S. Tamura, "Image guidance of breast cancer surgery using 3-D ultrasound images and augmented reality visualization," *IEEE Trans. Med. Imag.*, vol. 17, pp. 681–693, Oct. 1998.

[5] R. Rohling, A. Gee, and L. Berman, "Three-dimensional spatial compounding of ultrasound images," *Med. Image Anal.*, vol. 1, no. 3, pp. 177–193, 1997.

[6] A. Moskalik, P. L. Carson, C. R. Meyer, J. B. Fowlkes, J. B. Rubin, and M. A. Roubidoux, "Registration of three-dimensional compound ultrasound scans of the breast for refraction and motion correction," *Ultrasound Med. Biol.*, vol. 21, no. 6, pp. 769–778, 1995.

[7] G. Xiao, M. Brady, J. A. Noble, and M. Burcher, "Non-rigid registration in 3D free-hand ultrasound imaging of the breast," in *Proc. Computer Assisted Radiology and Surgery (CARS) 2001*, 2001, p. 1131.

[8] L. Brown, "A survey of image registration techniques," *Computing Surveys*, vol. 24, no. 4, pp. 325–376, 1992.

[9] J. B. A. Maintz and M. A. Viergever, "A survey of medical imaging registration," *Med. Image Anal.*, vol. 2, no. 1, pp. 1–36, 1998.

[10] G. E. Christensen, R. D. Rabbitt, and M. I. Miller, "Deformable templates using large deformation kinematics," *IEEE Trans. Image Processing*, pp. 1435–1447, May 1996.

[11] M. Bro-Nielsen and C. Gramkow, "Fast fluid registration of medical images," in *Lecture Notes in Computer Science*, vol. 1131, Proc. Visualization in Biomedical Computing. Berlin, Germany, 1996, pp. 267–276.

[12] J. P. Thirion, "Image matching as a diffusion process: An analogy with Maxwell's demons," *Med. Image Anal.*, vol. 2, no. 3, pp. 243–260, 1998.

[13] D. Rueckert, L. I. Sonoda, C. Hayes, D. L. G. Hill, M. O. Leach, and D. J. Hawkes, "Nonrigid registration using free-form deformations: Application to breast MR images," *IEEE Trans. Med. Imag.*, vol. 18, pp. 712–721, Aug. 1999.

[14] D. Aiger and D. Cohen-Or, "Mosaicing ultrasonic volumes for visual simulation," *IEEE Comput. Graph. Applicat.*, vol. 20, pp. 53–61, Mar.-Apr. 2000.

[15] J. F. Krücker, C. R. Meyer, G. L. LeCarpentier, J. B. Fowlkes, and P. L. Carson, "3D spatial compounding of ultrasound images using image-based nonrigid registration," *Ultrasound Med. Biol.*, vol. 26, no. 9, pp. 1475–1488, 2000.

[16] D. Collins and A. Evans, "Animal: Validation and applications of nonlinear registration-based segmentation," *Int. J. Pattern Recogn. Artif. Intell.*, vol. 11, pp. 1271–1294, 1997.

[17] P. Cachier and X. Pennec, "3D nonrigid registration by gradient descent on a Gaussian-windowed similarity measure using convolutions," in *Proc. IEEE Workshop Mathematical Methods in Biomedical Image Analysis*, 2000, pp. 182–189.

[18] P. M. Hayton, M. Brady, S. M. Smith, and N. Moore, "A nonrigid registration algorithm for dynamic breast MR images," *Artif. Intell.*, vol. 114, pp. 125–156, 1999.

[19] S. Prima, S. Ourselin, and N. Ayache, "Computation of the Mid-Sagittal Plane in 3D Medical Images of the Head," INRIA, France, Tech. Rep. 3841, 1999.

[20] F. Yeung, S. F. Levinson, and K. J. Parker, "Multilevel and motion model-based ultrasonic speckle tracking algorithms," *Ultrasound Med. Biol.*, vol. 24, no. 3, pp. 427–441, 1998.

[21] B. K. P. Horn and B. G. Schunk, "Determining optical flow," *Artif. Intell.*, vol. 17, pp. 185–203, 1981.

[22] J. Declerck, J. Feldmar, M. L. Goris, and F. Betting, "Automatic registration and alignment on a template of cardiac stress and rest reoriented spect images," *IEEE Trans. Med. Imag.*, vol. 16, pp. 727–737, Dec. 1997.

[23] G. Xiao, "3-D free-hand ultrasound imaging of the breast," Ph.D. dissertation, Dept. Eng. Sci., Oxford Univ., Oxford, U.K., 2001.

[24] M. Burcher, L. Han, and J. A. Noble, "Deformation correction in ultrasound imaging using contact force measurements," in *Proc. IEEE Mathematical Methods Biomedical Image Analysis (MMBIA 2001)*, 2001, pp. 63–70.